journal of the mechanical behavior of biomedical materials 147 (2023) 106084

Contents lists available at ScienceDirect

Journal of the Mechanical Behavior of Biomedical Materials

journal homepage: www.elsevier.com/locate/jmbbm

Research paper

Highly lubricious SPMK-g-PEEK implant surfaces to facilitate rehydration of articular cartilage

Robert J. Elkington [a,*], Richard M. Hall [b], Andrew R. Beadling [a], Hemant Pandit [c], Michael G. Bryant [a]

[a] Institute of Functional Surfaces, Mechanical Engineering, University of Leeds, Leeds, LS2 9JT, Yorkshire, UK
[b] Institute of Thermofluids, Mechanical Engineering, University of Leeds, Leeds, LS2 9JT, Yorkshire, UK
[c] Leeds Institute of Rheumatic and Musculoskeletal Medicine, Chapel Allerton Hospital, Chapeltown Road, Leeds, LS7 4SA, Yorkshire, UK

ARTICLE INFO

Keywords:
Polymer brushes
Cartilage
Cartilage repair
Orthopaedic engineering
BioTribology

ABSTRACT

To enable long lasting osteochondral defect repairs which preserve the native function of synovial joint counter-face, it is essential to develop surfaces which are optimised to support healthy cartilage function by providing a hydrated, low friction and compliant sliding interface. PEEK surfaces were modified using a biocompatible 3-sulfopropyl methacrylate potassium salt (SPMK) through UV photo-polymerisation, resulting in a ~350 nm thick hydrophilic coating rich in hydrophilic anionic sulfonic acid groups. Characterisation was done through Fourier Transformed Infrared Spectroscopy, Focused Ion Beam Scanning Electron Microscopy, and Water Contact Angle measurements.

Using a Bruker UMT TriboLab, bovine cartilage sliding tests were conducted with real-time strain and shear force measurements, comparing untreated PEEK, SPMK functionalised PEEK (SPMK-g-PEEK), and Cobalt Chrome Molybdenum alloy. Tribological tests over 2.5 h at physiological loads (0.75 MPa) revealed that SPMK-g-PEEK maintains low friction ($\mu < 0.024$) and minimises equilibrium strain, significantly reducing forces on the cartilage interface. Post-test analysis showed no notable damage to the cartilage interfacing against the SPMK functionalised surfaces.

The application of a constitutive biphasic cartilage model to the experimental strain data reveals that SPMK surfaces increase the interfacial permeability of cartilage in sliding, facilitating fluid and strain recovery. Unlike previous demonstrations of sliding-induced tribological rehydration requiring specific hydrodynamic conditions, the SPMK-g-PEEK introduces a novel mode of tribological rehydration operating at low speeds and in a stationary contact area. SPMK-g-PEEK surfaces provide an enhanced cartilage counter-surface, which provides a highly hydrated and lubricious boundary layer along with supporting biphasic lubrication.

Soft polymer surface functionalisation of orthopaedic implant surfaces are a promising approach for minimally invasive synovial joint repair with an enhanced bioinspired polyelectrolyte interface for sliding against cartilage. These hydrophilic surface coatings offer an enabling technology for the next generation of focal cartilage repair and hemiarthroplasty implant surfaces.

1. Introduction

Osteochondral defects or cartilage lesions are reported in up to 61% of symptomatic knee arthroscopies (Hjelle et al., 2002; Curl et al., 1997). Current cartilage defect treatment options can be broadly classified into biologic options (microfracture, debridement, resorbable implants) or minimally invasive focal cartilage repair implants. Biologic solutions aim to stimulate regrowth of tissue but typically yield biomechanically inferior fibrocartilage or otherwise inconsistent integration with native healthy tissue and are generally considered unsuitable for patients over 50 due to inhibited capacity for tissue regrowth (Mollon et al., 2013; Hangody and Füles, 2003). For older patients or those with contraindications unsuitable for biologic repair solutions, treatment options remain limited with total knee replacement (TKR) reserved for severe symptomatic osteoarthritis. TKR in patients under 60 are associated with a greater risk of revision, periprosthetic joint infection and aseptic mechanical failure (Bayliss et al., 2017; Meehan et al., 2014). Therefore, for middle-aged patients with full-thickness symptomatic cartilage defects, efforts are being made to address the treatment gap through the utilisation of a variety of less invasive, tissue-preserving focal cartilage repair implants.

* Corresponding author.
E-mail address: mnrje@leeds.ac.uk (R.J. Elkington).

https://doi.org/10.1016/j.jmbbm.2023.106084
Received 27 June 2023; Received in revised form 16 August 2023; Accepted 20 August 2023
Available online 25 August 2023

Focal articular prosthetic resurfacing devices are an emerging class of medical devices for the treatment of cartilage defects. Whilst ongoing clinical studies claim to show promising results, the current use of hard biomaterials in focal repair implants such as, cobalt–chromium alloy (CoCr) and ceramics, can quickly erode and overload the mating cartilage leading to pain, stiffness, and loss of function (Pawaskar et al., 2011; Kim et al., 2012; Willing et al., 2015; Adenikinju et al., 2019). The 2013 Australian joint registry reported that for partial knee resurfacing using a CoCr HemiCAP (Ortotech) the five year revision rate was 26.4%, most commonly due to disease progression (58.7%) and loosening (15.2%) (Jermin et al., 2015). Furthermore, concerns around tribocorrosion of CoCrMo surfaces and Co and Cr ion interactions with mating cartilage surfaces has been raised by Stojanovic et al. contributing to the current EUs narrative around the use of Co and Cr containing implants (Stojanović et al., 2019; Eichenbaum et al., 2021). *In vitro* mechanical assessment of CoCr focal repair implants against cartilage exhibit deleterious wear on the interfacing articular cartilage due to high contact loads leading to high wear (Diermeier et al., 2020; Custers et al., 2010). Hence, there is a clear need for a new generation of low stiffness materials for focal osteochondral lesion repair designed to support the natural function of opposing cartilage surfaces. Furthermore, implant designs which interface directly with cartilage should be designed to mimic the natural physiological tribological and poroelastic cartilage properties and maintain a high degree of fluid load support (Tan et al., 2023). To this end, biomimetic materials and physiologically relevant mechanical testing against cartilage sample should be investigated to inform the next generation cartilage optimised bearing materials, leveraging the current understanding of cartilage tribology.

The tribological properties of healthy cartilage in synovial joints are unparallelled by engineered materials, they are able to support loads of up to 10 times human body weight, with friction coefficients < 0.03, and can last a full lifetime (80+ years) showing little or no wear (Clarke et al., 1974; Unsworth et al., 1975; Roberts et al., 1982; Mabuchi et al., 1994; Dowson et al., 1975). Loading conditions in a human synovial joint can be highly variable, with an average stress window of 0.1–5 MPa and peak stresses of up to 10 MPa (Hodge and Harris, 1986; Adams and Swanson, 1985; Conzen and Eckstein, 2000; Stormont et al., 1985). Lubrication in a synovial joint is facilitated by the soft poroelastic 2–4 mm thick cartilage (Stewart, 2010; de Boer et al., 2020). By wet weight cartilage is approximately 80% water, 18% fibrous matrix proteins (mainly collagen and proteoglycans) and 2% chondrocytes (Sophia Fox et al., 2009).

Whilst the exact mechanisms of synovial lubrication are still debated, it is largely agreed that the impressive tribological properties of cartilage is, in part, due to its biphasic properties and interstitial fluid load support facilitated through the deformable, high permeability collagen matrix (de Boer et al., 2020; Burris and Moore, 2017; Moore and Burris, 2017). It has been shown that up to approximately of 90% of the joint load can be borne by interstitial fluid pressure, shielding the collagen matrix from overloading and subsequent damage (Krishnan et al., 2004; Ateshian, 1997). Cartilage is a dynamic system requiring interstitial fluid pressurisation to recover and respond to loading conditions during joint articulation (Voinier et al., 2022). Under loading fluid is exuded from cartilage until a fluid–solid pressure equilibrium is reached. Moore and co-workers have shown, through simultaneous measurement of friction force and cartilage strain, that the coefficient of friction of cartilage–glass contacts to be strain-dependent with high strains linked with higher coefficient of friction due to fluid exudation (Burris and Moore, 2017; Moore and Burris, 2017). The conformal geometry of the articulating joints facilitate *tribological rehydration* whereby sufficient hydrodynamic pressures are generated that can imbibe fluid into the cartilage to maintain a fluid pressure equilibrium (Voinier et al., 2022; Burris and Moore, 2017; Moore and Burris, 2017; Kupratis et al., 2021). However, these fluid–structure mechanisms only partially elucidate the impressive tribological properties of cartilage. The superficial surface of cartilage is composed of a supramolecular complex consisting of hydrophilic macromolecules found in synovial fluid. These include biopolyelectrolyte macromolecules hyaluronic acid (HA), and specialist lubricating glycoproteins, lubricin and aggrecan, along with surface active phospholipids (Dedinaite, 2012; Jahn and Klein, 2018). These molecules contain hydrophilic domains which sustain a self healing sliding interface enabled by tenaciously bound hydration shells on the charged macromolecules and hydrophilic phospholipids and described by the hydration lubrication model proposed by Klein Jahn and Klein (2015, 2018), Jahn et al. (2016).

Bioinspired cartilage lubrication strategies are an active area of research primarily exploring the use of polymers and manufacturing processes including electrospinning, functional scaffolds, hydrogels and polymer brushes (Siddaiah and Menezes, 2016; Lin and Klein, 2022). The latter, polymer brushes, have already been incorporated into functionalised orthopaedic CoCrMo-on-UHMWPE hip replacement bearings. Whilst *in vitro* tests have shown polyelectrolyte-functionalised UHMWPE to be an effective method of improving lubricity and wear in aqueous environments, clinical observations suggest no functional benefit when compared to un-functionalised and other modern UHMWPE materials (Lanigan et al., 2018; Kyomoto et al., 2015). Various cationic, anionic, and zwitterionic monomer species grafted to medical device relevant substrates (e.g. CoCrMo and PEEK) using UV initiated atom transfer radical polymerisation (ATRP) have been demonstrated to exhibit high lubricity (friction coefficient < 0.05) at loads exceeding 10^2 MPa (Mocny and Klok, 2016).

3-sulfopropyl methacrylate potassium salt (SPMK) is a widely researched low cost highly lubricious biocompatible hydrated monomer with applications in artificial synovial fluid for biomimetic lubrication and surface modification of catheters to reduce infection and irritation (Lanigan et al., 2018; Liu et al., 2014). SPMK is also a promising candidate for surface modification of artificial joints to improve lubricity and an alternative to largely reported 2-methacryloyloxyethyl phosphorylcholine (MPC) functionalised surfaces (Biresaw, 2013; Chouwatat et al., 2017; Elkington et al., 2021). As such, UV initiated polyelectrolyte functionalised surfaces offer a biomimetic surface treatment that replicates the large hydrophilic domained biomolecules found on the surface of cartilage with industrial scalability (Ishihara, 2022; Chen et al., 2007).

In light of the ageing and more active global population and the growing demand for TKR, which brings an associated revision burden, in a younger and more active demographic, there is a clear need for new technologies which (1) enable earlier and bone preserving interventions, (2) maintain and promote dynamic hydration–rehydration and tissue health of opposing cartilage surfaces and (3) provide scope and flexibility to be delivered with minimally invasive intervention. The aim of this study was to develop and demonstrate low trauma, low friction, Co and Cr free surfaces as an alternative to the current CoCrMo surfaces used in the current generation of focal implant designs. SPMK-g-PEEK surfaces were been prepared via UV initiated polymerisation and their biotribological performance were characterised.

Research into polyelectrolyte functionalised surfaces against cartilage remains limited, with Ishihara demonstrating MPC coated CoCrMo sliding against cartilage sustains low friction coefficients of < 0.01 and does not noticeably damage cartilage surfaces (Kyomoto et al., 2010a). However, the majority of work in this area focuses on applications in the acetabulum interface of total hip replacements, and principally elucidates the favourable lubrication properties of polyelectrolyte surfaces as enabled by the zwitterionic functional groups which provide a highly hydrated sliding interface (Kyomoto et al., 2010b; Ishihara, 2015b). Further mechanistic insight into how polyelectrolyte surface treatments can support native cartilage function is required.

Our hypothesis is that hydrated SPMK-g-PEEK surfaces will enable surfaces capable of sustaining and promoting effective hydration lubrication at cartilage interfaces. By promoting hydration and dissipating friction, cartilage trauma can be mitigated by supporting the natural modes of lubrication and interstitial fluid load support.

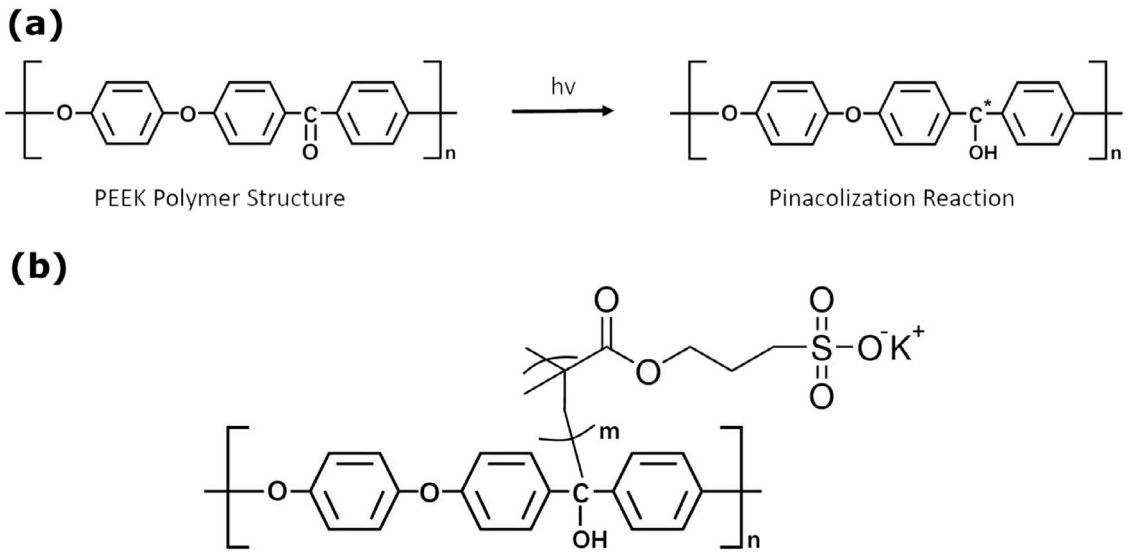

Fig. 1. (a) A benzophenone unit exposed to ultraviolet irradiation a pinacolization reaction is induced, forming a semi-benzopinocal (ketyl) radical that acts as a photoinitiator. (b) SPMK-grafted-PEEK achieved through grafting-to of the SPMK monomer showing the anionic sulfonic functional group.

2. Materials and methodology

This study will investigate the tribological performance of a SPMK polyelectrolyte functionalised PEEK (SPMK-g-PEEK) surface will be investigated, comparing it to unfunctionalised PEEK and CoCr surfaces, when interacting with articular cartilage under physiological loads. Coefficient of friction (CoF) and real time strain measurement will be used to analyse the cartilage response sliding against SPMK-g-PEEK. Low CoF will demonstrate effective hydration lubrication, whilst a reduced cartilage equilibrium strain compared to an unfunctionalised PEEK control will evidence enhanced fluid load support. Following testing, cartilage samples will be examined to quantify wear along with evidence of cartilage fibrillation or damage to the collagen matrix, indicating a breakdown in fluid load support. Ultimately, this study aims to evaluate the performance of SPMK-g-PEEK and its suitability for supporting physiological synovial tribology, specifically aimed at sustained lubricity and improved fluid load support in cartilage.

2.1. Materials

Victrex PEEK 450G was purchased from RS Components (UK) as a flat 5 mm thick sheet and cut into square samples of 25 × 25 mm. Surgical implant grade cobalt chrome alloy bar conforming to ASTM F1537-20 was purchased from Oracle Special Metals Ltd (Berkshire, UK).

Each PEEK and CoCr sample was polished to an R_a of 30 nm through successive grinding against P240, P400, P800 and P1200 grit paper followed by successive napless polishing using 3, 1, 0.5, 0.25 and 0.04 μm diamond and silica oxide suspensions. Sample roughness was validated post polishing using a Talysurf PGI NOVUS profilometer.

The monomer 3-sulfopropyl methacrylate potassium salt (SPMK, CAS No. 31098-21-2) in powder form, with a purity of greater than 98%, and phosphate buffered saline tablets (Product No. 524650) were purchased from Sigma Aldrich (UK) and used as received

Flat 7.2 mm diameter cartilage plugs were obtained from the patellofemoral groove of bovines slaughtered at approximately 2 years old (John Penny & Sons, Leeds, UK). Plug extraction was performed using an 8 mm trephine in a high speed 30,000 rpm rotary tool. During drilling a steady stream of phosphate buffered saline was used to ensure cartilage plugs were not damaged due to frictional heating.

Following harvesting any cartilage plugs with a slanted or convex surface were discarded, retaining only flat plug geometries determined by placing the surface section against a transparent rule. Cartilage plugs were washed and stored frozen at –18 °C in phosphate buffer saline (PBS), samples were defrosted 24 h before use and brought up to room temperature before testing. Single cycles of freezing and thawing have demonstrated no difference in tribological properties compared to fresh articular cartilage samples (Forster and Fisher, 1999). The osmolarity and ion concentrations of PBS emulates the isotonic body fluid environment which provides a suitable storage and immersion fluid for cartilage to prevent cartilage swelling, deformation, and maintain tissue hydration, it is routinely used during *in vitro* cartilage tribological testing (Chan et al., 2011; Burris et al., 2019)

2.2. Hydrophilic functionalisation of PEEK

SPMK functionalised PEEK samples were prepared with reference to the method developed by Kobayashi for MPC (Kobayashi and Takahara, 2010, 2012). Polished PEEK samples were washed in acetone for 30 min in an ultrasonic bath, washed with isopropanol, and then dried in a stream of air. SPMK aqueous solution was prepared at a 1 $molL^{-1}$ concentration and purged with nitrogen for 2 h to remove oxygen. In a glove box flooded with nitrogen cleaned PEEK substrates were immersed in the SPMK solution and exposed to 5 $mWcm^{-2}$ ultraviolet (UV) light at a 365 nm wavelength (Analytik Jena UVP Crosslinker CL-3000L) for 90 min for a total UV exposure of 27 Jcm^{-2}. Following photopolymerisation, functionalised PEEK samples were washed with isopropanol and deionised water to remove excess unreacted monomer.

Hydrophilic surfaces can be prepared through surface initiated polymerisation using a grafting-from approach of polymerising SPMK monomer onto PEEK substrates. PEEK comprises of an aromatic backbone molecular chain with ketone and ether functional groups. The presence of a benzophenone unit (an aryl ketone) in the molecular structure, which when irradiated by UV undergoes a pinacolization reaction to form a semi-benzopinocal radical (i.e. ketyl radicals) which act as a photoinitiator as shown in Fig. 1(a). This can be exploited for self initiated surface graft polymerisation enabling direct grafting of functional SPMK polymers onto the PEEK surface without using a photoinitiator (Nakano et al., 2020). Anionic sulfonic acid groups (Fig. 1(b)) in the SPMK structure have a high affinity for water and in aqueous conditions provide a highly hydrated lubricious soft interface (Kobayashi and Takahara, 2012).

2.3. FTIR

Fourier Transformed Infrared Spectroscopy with an attenuated total reflection module (FTIR-ATR) was performed using a Spotlight 400 (Perkin Elmer, Massachusetts USA) to confirm the presence of grafted polymer following UV initiated photopolymerisation.

IR spectra were obtained from 16 scans with four repeats at four different locations on each grafted PEEK surface between 650–4000 cm^{-1} at a resolution of 4 cm^{-1}. Transmittance profiles were then compared to SpectraBase FTIR-ATR database to confirm the presence of SPMK on the PEEK surface.

2.4. Wettability

Water contact angle (WCA) measurement were performed by dropping 10 μL of purified Milli-Q water from a fixed height of 40 mm onto the sample surface all in ambient temperatures (298 K). After allowing the water droplet to wet the surface and become static for 30 s, the droplet is illuminated using an Attension Theta Tensiometer (Nanoscale Instruments, Phoenix, USA) producing a high contrast image of the droplet imaged with a CMOS camera. Attension Theta software was used to determine the water contact angle in air. Each measurement was repeated 5 times to calculate an average WCA measurement.

2.5. Focused ion beam-scanning electron microscopy

A Helios G4 CX Dual Beam (FEI, USA) Scanning Electron Microscope (SEM) with a precise Focussed Ion Beam (FIB) was used to measure the dry film thickness of the SPMK grafted PEEK surfaces.

Prior to analysis, samples were dehydrated in a vacuum and coated with a 20 nm of iridium. Samples were then placed in the FIB-SEM microscope and a layer of platinum was deposited on the surface via an electron and ion beam. Both of these processes were necessary to ensure the SPMK surface would be preserved throughout the gallium ion beam FIB cross sectioning. A 3 × 10 × 10 μm section was milled to expose a cross section of the SPMK-g-PEEK interface which was then imaged under SEM to observe the dry film thickness. Two cross sections were taken on an SPMK-g-PEEK samples to enable a representative calculation of dry SPMK film thickness across the sample.

2.6. Mechanical testing

A Bruker UMT Tribolab fitted with a reciprocating linear drive and custom built lubricant bath was used to perform cartilage-pin on CoCr, PEEK, and SPMK-g-PEEK plates. Plate samples were fixed in the bath and cartilage pins were fixed to a rigid load and displacement transducer. During testing samples were fully submerged in PBS as an isotonic test fluid to simulate a physiological environment and subsequently mitigate cartilage swelling and maintain a hydrated equilibrium representative of an *in vivo* environment. A schematic of the experimental setup is shown in Fig. 2a.

Throughout testing closed loop control enabled simultaneous measurement of the Coefficient of Friction (μ) and cartilage compressive strain (ε):

$$\mu = \frac{F_x}{F_z} \tag{1}$$

$$\varepsilon = \frac{\Delta h}{h} \times (100\%) \tag{2}$$

where F_x and F_z are the measured forces in the tangential (**x**) and normal (**z**) directions respectively, h is the baseline full thickness of the cartilage, and Δh is the compressed cartilage height.

Throughout testing a constant normal load (F_z) of 30 ± 3 N is applied and maintained with PID control. This corresponds to a physiologically representative spatially averaged contact pressure of approximately 0.75 MPa for human hip and tibiofemoral joints (Hodge and Harris, 1986; Brand, 2005).

Table 1
Compression-Sliding test parameters for SPMK-g-PEEK, PEEK, and CoCr tests. All tests lasted 9000 s with a constant applied load of 30 N, constant speed of 10 mms^{-1} and total sliding distance of 90 m.

	SPMK-g-PEEK	PEEK	CoCr
Load	30 N	30 N	30 N
Speed	10 mm/s	10 mm/s	10 mm/s
Reciprocating distance	20 mm	20 mm	10 mm
Test length	9000 s	9000 s	9000 s
Total sliding distance	90 m	90 m	90 m

Fig. 2(b) show the two 150 min testing regimes employed. Unconfined compression of a constant applied 30 N load for 150 min and the time dependent strain response of cartilage is recorded against PEEK, SPMK-g-PEEK, and CoCr (each n = 3).

Table 1 summarises the compression-sliding routines which applied a constant load of 30 N throughout a 9000 s test of cartilage pin-on-plate reciprocating sliding. SPMK-g-PEEK (n = 4) and PEEK (n = 4) plates were slid against cartilage pins with a 20 mm stroke length for 2250 cycles. The smaller 25 mm diameter CoCr plates (n = 3) underwent sliding with a 10 mm stroke length for 4500 cycles. The sliding stage underwent a sawtooth displacement profile, as such the velocity profile consisted of alternating periods of constant positive and negative velocities at a speed of 10 mms^{-1}. For each sample test this equates to a total sliding distance of 90 m.

The unconfined compression tests serve as a baseline measurement of cartilage strain without any sliding induced rehydration. The compression-sliding data can then be directly compared to the strain responses of the pin-on-plate sliding tests using the same contact geometry to quantify sliding induced cartilage rehydration.

Coefficient of Friction (CoF), μ, and strain, ε, are reported as a single average value for each reciprocating cycle. Both values are calculated from the mid 50% of the reciprocating cycle, with the value from each cycle calculated from the mean of the forward and backward stroke, in order to calculate CoF during steady state sliding.

The strain response of cartilage throughout mechanical testing was fitted using a custom script written in Python 3.7 to understand the viscoelastic time dependent creep by fitting to the biphasic theory equation (Mow et al., 1980). All mathematical code was written using scripts enabled by pandas, NumPy along with curve fitting using SciPy non-linear least squares fit algorithm (Virtanen et al., 2020).

2.7. Cartilage surface analysis

Following testing cartilage pins were stored in 10% neutral buffered formalin using CellPath CellStor Pre-filled Specimen Containers at room temperature. Prior to analysis cartilage samples were washed and soaked thoroughly in phosphate buffered saline. Measurement of the cartilage height was performed on a Keyence VHX-7000 with a 20× magnification calibrated with a reference scale accurate to ±0.1 μm, enabling accurate pixel measurements to be taken on sample images. Four images were taken of each cartilage plug of the transverse plane, with the cartilage plug rotated about its long axis of symmetry by 90° between each image. This generated a set of four images which show the full 360° of the cartilage layer height. Using Keyence measurement software the line of best fit was plotted along the tidemark (calcified cartilage–bone interface) along with the top surface of the cartilage, the average cartilage height between the fitted lines is then calculated. Cartilage height is calculated from the average of the four images taken per sample. An annotated image demonstrating the measurement procedure is shown in Fig. 3.

Accutrans (a casting silicone used for taking transfer moulds) replicas of the cartilage plug surface were analysed using an Infinite Focus Optical 3D Measurement Microscope (Alicona, USA). Macroscopic images were taken over the entire surface of the plug to identify

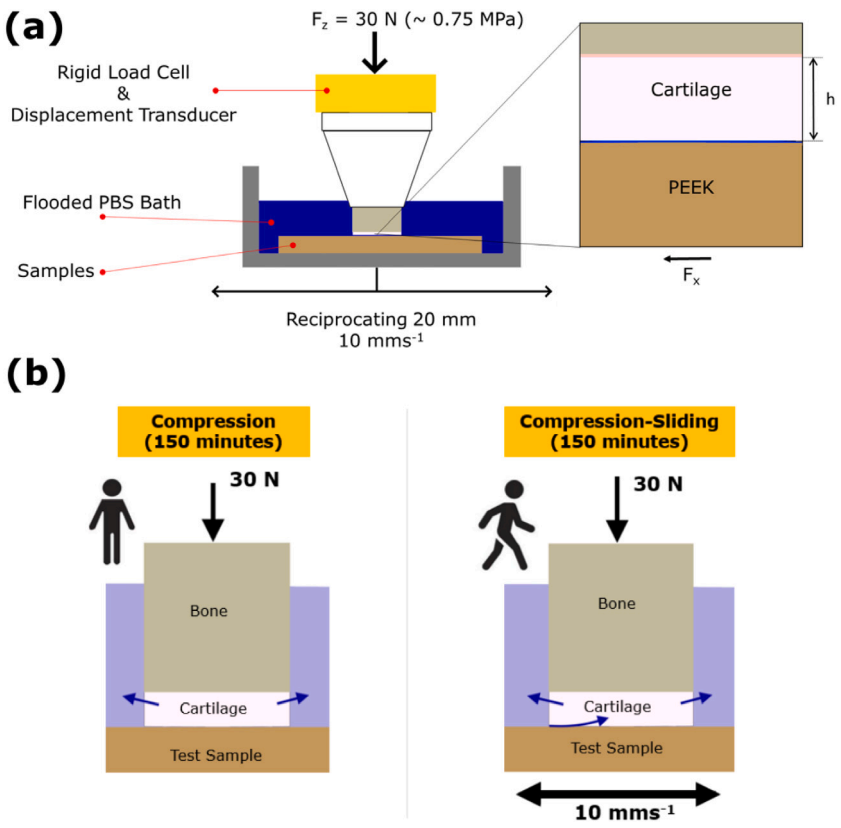

Fig. 2. (a) Schematic of cartilage pin on plate testing on the Bruker UMT (b) the testing regimes employed in the study: compression where a 30 N load is applied and held for 150 min and compression-sliding where a 30 N load is applied with a reciprocating sliding speed of 10 mms^{-1}.

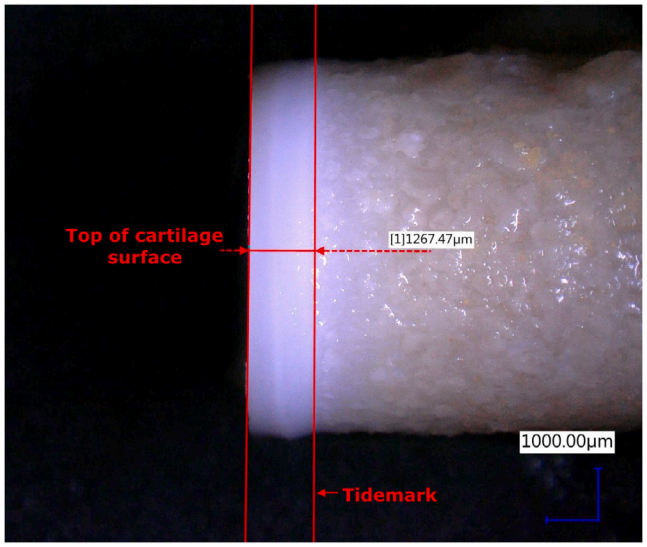

Fig. 3. Measurement of cartilage layer height using images taken on a Keyence VHX-7000 analysed using the supplied Keyence measurement suite.

significant wear artefacts and fibrillation. Additionally, microscale measurements over an area of 0.5 mm width across the centre of the cartilage plugs determine the roughness of the cartilage indicating surface degradation.

Roughness measurements were taken on the cartilage sample after undergoing sliding against PEEK, SPMK-g-PEEK and CoCr, along with unused fresh cartilage plugs as a control. Roughness profiles were taken over the central 4 mm of each cartilage plug, a cut off filter with a wavelength of 250 µm was used to remove profile features caused by bubbles in the silicone moulds or the uneven geometry of natural cartilage. For each of the sliding counter-face materials, an average value of the cartilage roughness following sliding was calculated.

3. Results

3.1. FTIR-ATR

Fig. 4 shows the FTIR-ATR spectra of unfunctionalised PEEK and SPMK-g-PEEK samples. CoCr is not included as it did not include any notable IR absorption peaks. IR absorption peaks for the ester carbonyl group C=O (1721 cm^{-1}) and sulfonate group S=O (1045 cm^{-1}) are clearly observed, indicating successful UV initiated polymer grafting of SPMK to the PEEK substrate (Chouwatat et al., 2017). A broad adsorption peak around 3400 cm^{-1} also indicates water bound at the hydrophilic sulfonic acid groups of the SPMK (Lanigan et al., 2018).

3.2. Water contact angle

Static water contact angle (WCA) measurements shown in Fig. 5 demonstrate that SPMK functionalisation is able to modify the surface wettability of a hydrophobic PEEK substrate, substantially enhancing the hydrophilic properties. PEEK and CoCr yielded higher WCA of 82.7° ±2.2° and 76.7° ±6.2° respectively corresponding to a hydrophobic surface eliciting a low surface energy. SPMK-g-PEEK had a static WCA of 33.5° ±3.1° demonstrating a high surface energy and affinity for water, providing an interface optimised for retaining a fluid film in an aqueous environments (Law, 2014; Kobayashi and Takahara, 2010, 2012). A decrease of 49.2° of WCA was observed between PEEK versus SPMK-g-SPMK.

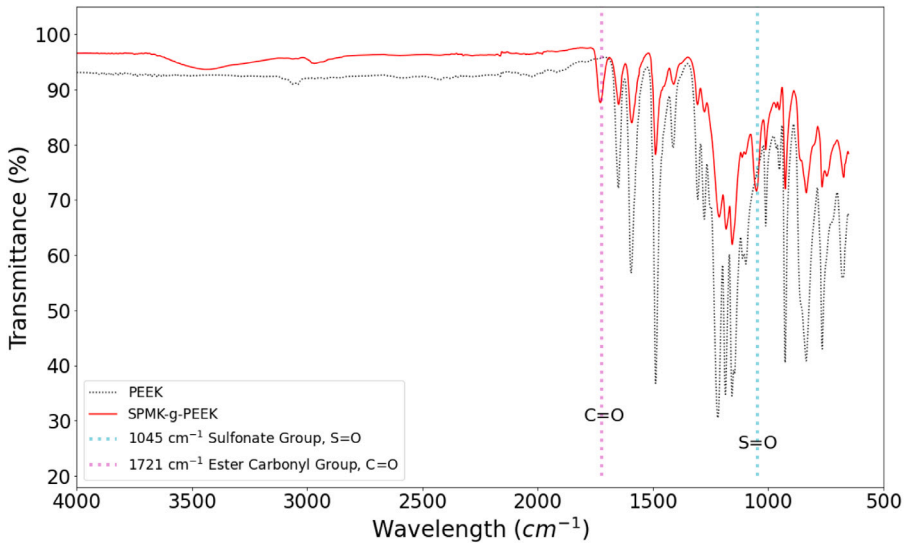

Fig. 4. FTIR-ATR Spectra of unfunctionalised PEEK and SPMK-g-PEEK with IR absorption peaks for ester carbonyl and sulfonate groups shown.

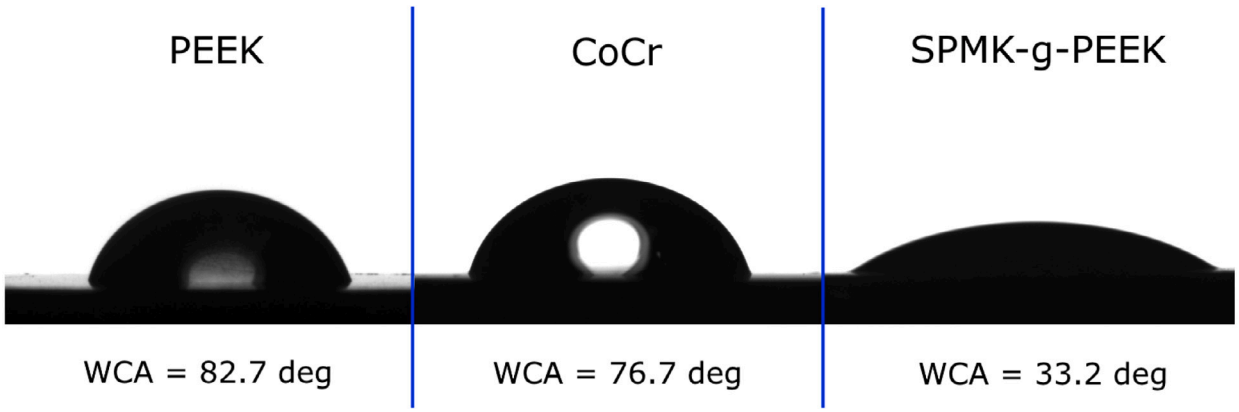

Fig. 5. Static water contact angle (WCA) images and measurements for unfunctionalised PEEK 82.7° ±2.2° (n = 5), CoCr 6.7° ±6.2° (n = 5), and SPMK-g-PEEK 33.5° ±3.1° (n = 5).

3.3. FIB-SEM dry film thickness

Fig. 6 show the FIB-SEM cross section and dry layer thickness of SPMK-g-PEEK surfaces. An average dry film thickness of 397 ± 47 nm (n = 8) was observed on SPMK-g-PEEK samples. FIB-SEM also indicated a layer of uniform thickness and distribution across the surfaces within the area analysed. The 'crackled' surface appearance is attributed to dehydration (under UHV) and application of the protective Platinum layer.

3.4. Continuous pin-on-plate sliding

The evolution of CoF during sliding is shown in Fig. 7(a). PEEK and CoCr surfaces slid against a static cartilage pin exhibited an increasing CoF up to a high final CoF (μ_{final}) of 0.45 ± 0.04 and 0.35 ± 0.04 respectively at the end of the test. In contrast, SPMK-g-PEEK maintained a low CoF throughout the test duration increasing monotonically to μ_{final} of 0.024 ± 0.01. The startup CoF $\mu_{startup}$ (t = 1 s) and final CoF μ_{final}v (t = 9000 s) are summarised in Table 2.

Fig. 7(b) show the cartilage strain evolution for the Compression and Compression-Sliding experiments. This was characterised by an initial rapid increase in strain where interstitial fluid is rapidly exude from the cartilage (t < 3600 s), followed by a steadier creep towards strain equilibrium.

For the Compression tests no sliding induced rehydration of the cartilage plug is possible, and benchmarks the maximum expected fluid exudation and final cartilage strain response after 9000 s of loading. For unconfined compression a typical biphasic creep response was observed with average values for PEEK ε_{max} of 49.7 ± 7.8%, SPMK-g-PEEK ε_{max} of 55.0 ± 5.4% and CoCr ε_{max} of 59.6 ± 12%. Each value is summarised in Table 2. When considering the uncertainty in each dataset it can be concluded that the strain response for cartilage with no sliding reduce rehydration broadly yields an equilibrium strain of ~ 45%–65% ε_{max}.

In-situ cartilage strain measurement during the Compression-Sliding tests presented a similar monotonic relationship. The final strain ε_{max} for PEEK and CoCr was 52.5 ± 7.5% and 39.8 ± 5.0% respectively. SPMK-g-PEEK yielded the lowest ε_{max} of 26.3 ± 7.6%, demonstrating functionalisation of PEEK surfaces with SPMK is able to effectively halve the equilibrium strain when sliding against cartilage.

3.5. Cartilage surface analysis

Figs. 8 show Accutrans moulds taken of cartilage pin surfaces for sliding against (a) PEEK (b) SPMK-g-PEEK and (c) CoCr surfaces respectively. Analysis of cartilage pins sliding against PEEK show deep scratches and fibrillation in the surface, tearing of the cartilage surface is due to high shear forces at the interface during testing. No notable scratches or fibrillation were observed on the cartilage surface interfacing with SPMK-g-PEEK or CoCr samples.

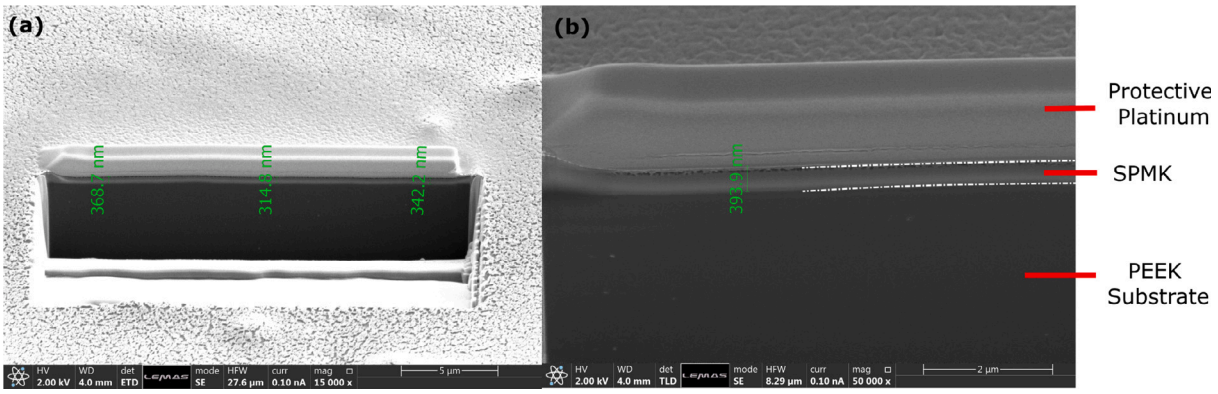

Fig. 6. FIB-SEM cross section images of SPMK-g-PEEK showing (a) milled section for analysis which enabled measurement of the dry SPMK layer height using SEM at 15,000× and (b) 50,000× magnification with annotation on material conformation of analysed surface. Green markings demonstrate measurement of local SPMK layer thickness on the PEEK substrate.

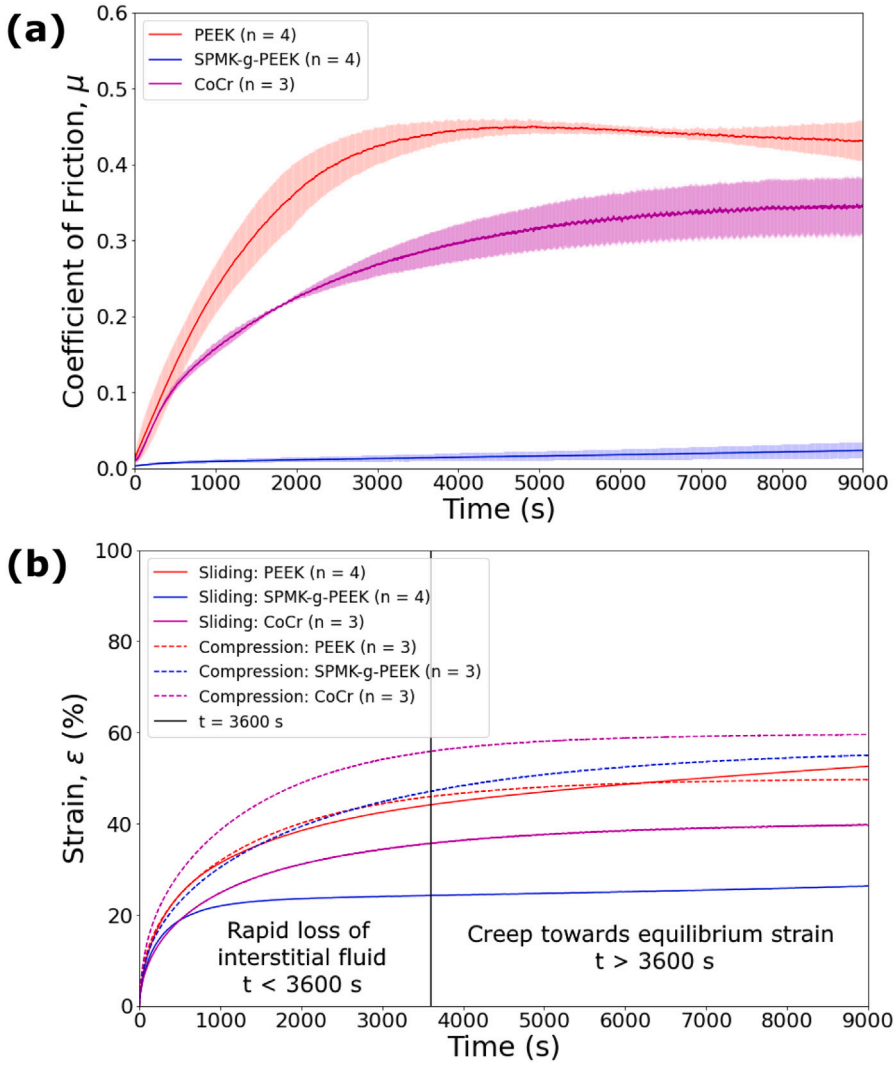

Fig. 7. (a) Dynamic friction per reciprocating sliding cycle for a cartilage pin sliding against PEEK, SPMK-g-PEEK, and CoCr under a constant 30 N load, 20 mm reciprocating distance at a speed of 10 mms^{-1}. Error bars shown standard deviation in each reciprocating cycle for each material data set. (b) Compression and Compression-Sliding (mean strain per reciprocating sliding cycle) for cartilage against PEEK, SPMK-g-PEEK and CoCr surfaces. Error bars are omitted for figure clarity, see Table 2.

For each test the mean average arithmetic roughness (R_a) and maximum valley height (R_z) are calculated to quantify cartilage surface fibrillation (roughness, R_a) and any localised tearing (R_z), summarised in Table 3. The largest features (maximum peak/valley height) were observed on the PEEK (Fig. 8(a)) samples corresponding to tearing in the cartilage surface. Broad peaks and valleys with large feature heights of 14.19 ±8.15 μm indicate significant damage to the cartilage, compared to an unused cartilage control with feature heights of 5.33

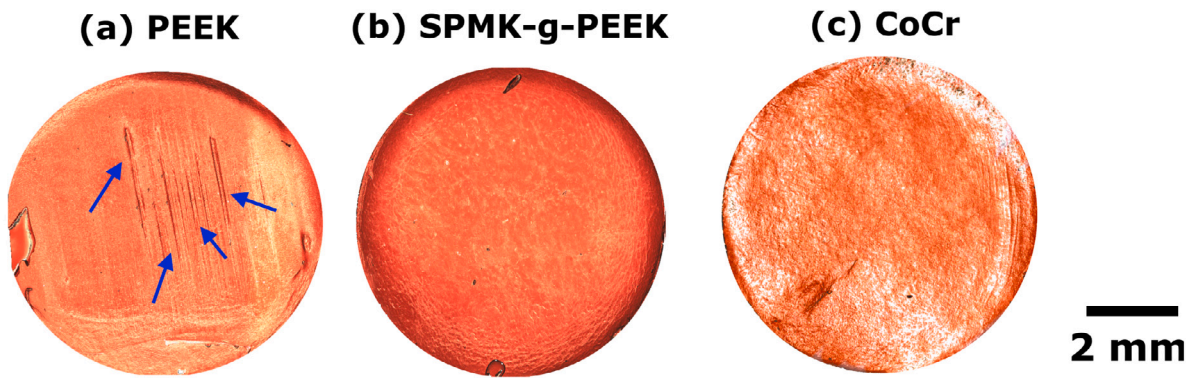

Fig. 8. Images of Accutrans moulds of cartilage pins following 9000 s sliding against (a) PEEK showing localised fissuring and fibrillation of cartilage surface marked with blue arrows and (b) SPMK-g-PEEK exhibiting no notable deleterious wear to cartilage surface and (c) CoCr showing evidence of surface fibrillation. For each sample, it should be noted that the appearance of blister like defects at the sample edges are air bubble artefacts during the Accutrans moulding process.

Table 2
Steady state CoF and final strain (ε_{max}) after 9000 s sliding against cartilage for the PEEK, CoCr, and SPMK-g-PEEK.

Sample	Compression	Compression-Sliding		
	Final strain ε_{max} (%)	Startup CoF $\mu_{startup}$ (t = 1 s)	Final CoF μ_{final} (t = 9000 s)	Final strain ε_{max} (%)
PEEK	49.7 ± 7.8 (n = 3)	0.020 ± 0.007	0.45 ± 0.04	52.5 ± 7.5 (n = 4)
SPMK-g-PEEK	55.0 ± 5.4 (n = 3)	0.003 ± 0.001	0.024 ± 0.01	26.3 ± 7.6 (n = 4)
CoCr	59.6 ± 12 (n = 3)	0.016 ± 0.005	0.35 ± 0.04	39.8 ± 5.0 (n = 3)

Table 3
Mean maximum valley height (R_z) and arithmetic roughness (R_a) measured for cartilage samples following sliding against PEEK, SPMK-g-PEEK, and CoCr, along with unused (fresh) cartilage control samples. Due to improper storage after testing, one CoCr interfacing cartilage plug was rendered unsuitable for post-testing surface analysis and roughness measurement.

Name	R_z/μm	R_a/μm
PEEK (n = 4)	14.19 ± 8.2	2.49 ± 0.52
SPMK-g-PEEK (n = 4)	2.70 ± 0.77	0.69 ± 0.16
CoCr (n = 2)	3.18 ± 1.0	0.64 ± 0.20
Fresh Cartilage (n = 3)	5.33 ± 0.54	1.04 ± 0.09

±0.54 μm. Similarly cartilage sliding against PEEK exhibits a increase in roughness with R_a values of 2.49 ±0.52 μm compared to the cartilage control with an R_a of 1.04 ±0.09 μm. Cartilage sliding on CoCr exhibited maximum feature heights of 3.18 ±1.01 μm and roughness values of 0.64 ±0.20 μm. Cartilage sliding on SPMK-g-PEEK samples yielded maximum feature heights and average roughness in the ranges of 2.70 ±0.77 μm and 0.69 ±0.16 μm respectively. Compared to the cartilage control, sliding against CoCr and SPMK-g-PEEK reduced the cartilage roughness, effectively flattening the rough profile of natural cartilage.

4. Discussion

Focal metallic cartilage resurfacing is an emerging clinical procedure that offers a solution between the biologic repair and total joint arthroplasty for active patients with early stage osteoarthritis and full-thickness cartilage defects. The advantages of this technique include local management of the defect retaining healthy tissues, maintaining joint stability with surfaces contoured to be congruent with the natural joint. However, osteoarthritis progression, persisting pain along with cartilage erosion and the subsequent high revision rate is common in the medium to long term. Strategies to reduce erosion and promote adjacent cartilage tissue health may enable better outcomes at the medium-long term.

4.1. Surface and tribological properties of SPMK-g-PEEK

PEEK substrates were successfully grafted with end tethered SPMK polyelectrolytes via surface initiated photopolymerisation induced by the benzophenone groups in PEEK. Following surface modification, FTIR-ATR confirmed successful grafting of SPMK-g-PEEK confirming the presence of anionic sulfonate functional groups. These functional groups play a crucial role in maintaining the polymer brush structure under high loads through electrostatic repulsive interactions and high affinity for water promote a highly hydrated interface in aqueous conditions (Kobayashi and Takahara, 2012; Lanigan et al., 2018). Water contact angle measurements demonstrate SPMK surface functionalisation reduces the PEEK WCA of 82.7° ±2.2° to a highly wettable WCA of 33.5° ±3.1° for SPMK-g-PEEK, essential for highly lubricious performance in aqueous environments.

The nanoscale layer thickness of the dry SPMK of 397 ± 47 nm determined by FIB-SEM measurements is approximately four times thicker than comparable applications of polyelectrolyte polymer brush functionalised surfaces developed by Ishihara Kyomoto et al. (2010b). Measurements of dry surface coatings of MPC on polyethylene are reported to be in the region of 80–100 using transmission electron microscopy on functionalised surface cross sections. MPC functionalised surfaces exhibit high lubricity in aqueous environments and have been incorporated into polyethylene acetabular cups in total hip replacement (Ishihara, 2015a; Goda et al., 2006). The significantly thicker dry film coating compared to those in the aforementioned studies raises questions about the exact polymer conformation at the surface and will be subject to further investigation.

Throughout sliding tests against cartilage, SPMK-g-PEEK sustained a low CoF ranging between 0.003–0.024 which are comparable to the CoF measured for healthy cartilage–cartilage interfaces. Cadaveric hip pendulum experiments designed to emulate gait have measured cartilage–cartilage contacts having a CoF in the range of 0.01–0.04 (Clarke et al., 1974; Unsworth et al., 1975; Dowson et al., 1975). Similarly, benchtop cartilage pin-on-plate tribometer tests at loads in the range of 0.2–0.4 MPa have demonstrated cartilage steady state

CoF in the range of 0.05–0.07 (Northwood and Fisher, 2007; Katta et al., 2007). Anionic polyelectrolyte surfaces are able to facilitate hydration lubrication, whereby tenaciously bound water molecules at the functional groups maintain a highly hydrated sliding interface (Chen et al., 2007; Lin and Klein, 2019). Through surface force balance observations based on synthetic end tethered polyelectrolytes, a lubrication mechanism enabled through hydration lubrication proposed by Klein hypothesises that boundary synovial lubrication can be attributed to hydration lubrication enabled by the hydrophilic macromolecule complexes (hyaluronic acid, aggrecan, and phospholipids) at the superficial cartilage interface which maintain a fluid like lubrication layer and dissipate friction via exchange of water ions between hydration shells (Jahn and Klein, 2015; Jahn et al., 2016; Chen et al., 2007).

In comparison, untreated PEEK (μ_{final} = 0.45) and CoCr (μ_{final} = 0.35) surfaces do not exhibit sustained hydration-enabled lubrication, resulting in rapid increases in CoF beyond levels observed in healthy cartilage–cartilage contacts. The lack of sustained lubrication in these materials can be attributed to their lower affinity for surface water as demonstrated by high water contact angles, especially in the case of PEEK, which exhibits the lowest surface energy. The improved wettability of CoCr compared to PEEK provides a slightly improved hydrophilic interface that can partially support lubrication at the interface (Pawlak et al., 2011). This allows for some degree of biphasic lubrication, which will maintain the hydration state of the interfacing cartilage. While the direct relationship between water contact angle and friction is not linear and remains a research gap, these factors collectively contribute to reducing the coefficient of friction at the cartilage–CoCr interface.

The interstitial fluid and pressure loss in cartilage under an applied load is closely linked to the changes in CoF. When the cartilage is initially loaded, the interstitial fluid pressure (IFP) plays a crucial role in supporting most of the applied load. However, as the load persists, the interstitial fluid is gradually exude out of the cartilage, leading to a transfer of load to the solid collagen matrix. This transition causes an increase in the CoF as both a higher load is transferred to the solid interface and weeping lubrication become diminished. After a sustained period of loading (i.e. t > 3600 s) almost all of the interstitial fluid is forced out of the cartilage, an equilibrium state of strain and CoF is reached where the load is primarily supported by the solid collagen matrix (Moore et al., 2017; Krishnan et al., 2004).

The study design, which involved using 7.2 mm diameter flat cartilage plugs, facilitated a static contact area and arrested tribological rehydration attributable to hydrodynamic wedge effects, enabling a more controlled analysis (Moore et al., 2017; Burris and Moore, 2017; Burris et al., 2019). Use of a stationary contact area enabled a direct comparison of sliding-compression tests to unconfined compression data, which benchmarks the time-dependent cartilage strain response.

Following 9000 s of unconfined compression against PEEK, an equilibrium strain (ε_{max}) of 49.7 ± 7.8% was observed, representing a state of maximal loss of interstitial fluid pressure (IFP) under a load of 30 N. In comparison, the equilibrium strain during sliding against PEEK was measured at 52.5 ± 7.5%, which, considering the strain error, indicates a comparable state of IFP loss. Cartilage sliding against CoCr demonstrated some extent of IFP was retained, with an ε_{max} of 39.8 ± 5.0%, approximately 20% lower than the total strain observed in the unconfined compression control. The wettability of CoCr provides a slightly improved hydrophilic interface to support lubrication. This also supports the hydration state of the interfacing cartilage, enabling some biphasic lubrication. While the direct link between WCA and friction is not linear, these factors together play a vital role in reducing the coefficient of friction on the CoCr surface.

One of the key findings of this study is the notable reduction in the equilibrium strain observed with SPMK-g-PEEK, with ε_{max} measured at 26.3 ± 7.6%. This represents a significant decrease of approximately 47% in the expected IFP loss compared to the unconfined compression control. These findings provide compelling evidence that SPMK polyelectrolyte functionalised surfaces are able to support sliding induced rehydration and modulate interstitial fluid flow, through a novel mechanism independent of hydrodynamic fluid inflow. The most likely explanation is the interplay of hydration lubrication and sustained biphasic fluid load support. The highly hydrophilic nature of the SPMK-g-PEEK surfaces provides a boundary lubricating layer, maintaining a low CoF at the interface. Additionally, the tenaciously bound hydrated species provide a hydrated region which, during sliding, facilitates the influx of fluid into the contact interface and its absorption into the cartilage surface.

Deleterious cartilage fibrillation was only observed in cartilage samples sliding against unfunctionalised PEEK and CoCr (Fig. 8) while no notable damage was found in pins sliding against SPMK-g-PEEK. Similarly, cartilage sliding against PEEK showed increased roughness (R_a) and valley height (R_z) compared to the fresh cartilage control and samples sliding against SPMK and CoCr (Table 3). The high CoF and strain behaviour during PEEK sliding demonstrates a total loss of IFP, leading to a situation where the majority of load in the contact is borne on the solid collagen phase leading to high shear forces and failure in the collagen fibre matrix.

4.2. Biphasic theory analysis

In the context of the presented minimised strain behaviour for SPMK-g-PEEK (Fig. 9), the application of biphasic theory analysis has been employed to elucidate and provide an explanation for the encouraging observations related to coefficient of friction (CoF), strain, and the mitigated cartilage damage achieved with SPMK-g-PEEK surfaces compared to unfunctionalised biomaterial surfaces. The flow-dependent viscoelastic behaviour of cartilage is commonly described using biphasic theory (Mow et al., 1980). This model for cartilage creep behaviour is shown in Eq. (3) which for a time constant τ the asymptotic creep towards strain equilibrium ($\varepsilon(t)$) can be described. The characteristic time constant τ_c quantifies the time to reaching creep equilibrium (Cutcliffe et al., 2020; Armstrong and Mow, 1982).

$$\varepsilon(t) = -\frac{\sigma}{H_A}\left[1 - 2\sum_{n=0}^{\infty}\frac{1}{M}e^{-\left(\frac{M}{\tau}\right)t}\right] \tag{3}$$

and

$$M = \pi^2\left(n + \frac{1}{2}\right)^2 \tag{4}$$

$$\tau = \frac{h^2}{H_A k} \tag{5}$$

where ε = strain, t = time, τ = time constant, τ_c = characteristic time constant, h = cartilage thickness, σ = applied stress, H_a = aggregate modulus, and k = permeability.

For quantitative temporal analysis of the time-dependent cartilage strain behaviour during the initial hour of biphasic creep (t < 3600 s, see Fig. 7(b)) a 5th order approximation (0 ≤ n < 5) of Eq. (3) is fitted to the strain data using a nonlinear least squares fit algorithm to calculate characteristic time constants (τ_c). A 5th order approximation was deemed suitable for fitting since $log(t_{max}/t_{min}) = log(9000/0.1) = 5.0$. This approximation was chosen because it sufficiently represents variations in the data without overcomplicating the model, as evidenced by the logarithmic ratio of the time data, which equals 5.0.

The quality of the curve fit is assessed through calculating the coefficient of determination, R-squared (R^2) using Eq. (6).

$$R^2 = 1 - \frac{\sum_t\left(\varepsilon_t - \varepsilon(t)\right)^2}{\sum_t\left(\varepsilon_t - \bar{\varepsilon}\right)^2} \tag{6}$$

Fig. 9 shows the fitting of the biphasic strain equation (Eq. (3)) to the strain response of cartilage samples during unconfined compression (no sliding) and sliding against PEEK, SPMK-g-PEEK and CoCr surfaces during the initial 3600 s of testing. Table 4 summarises the parameters

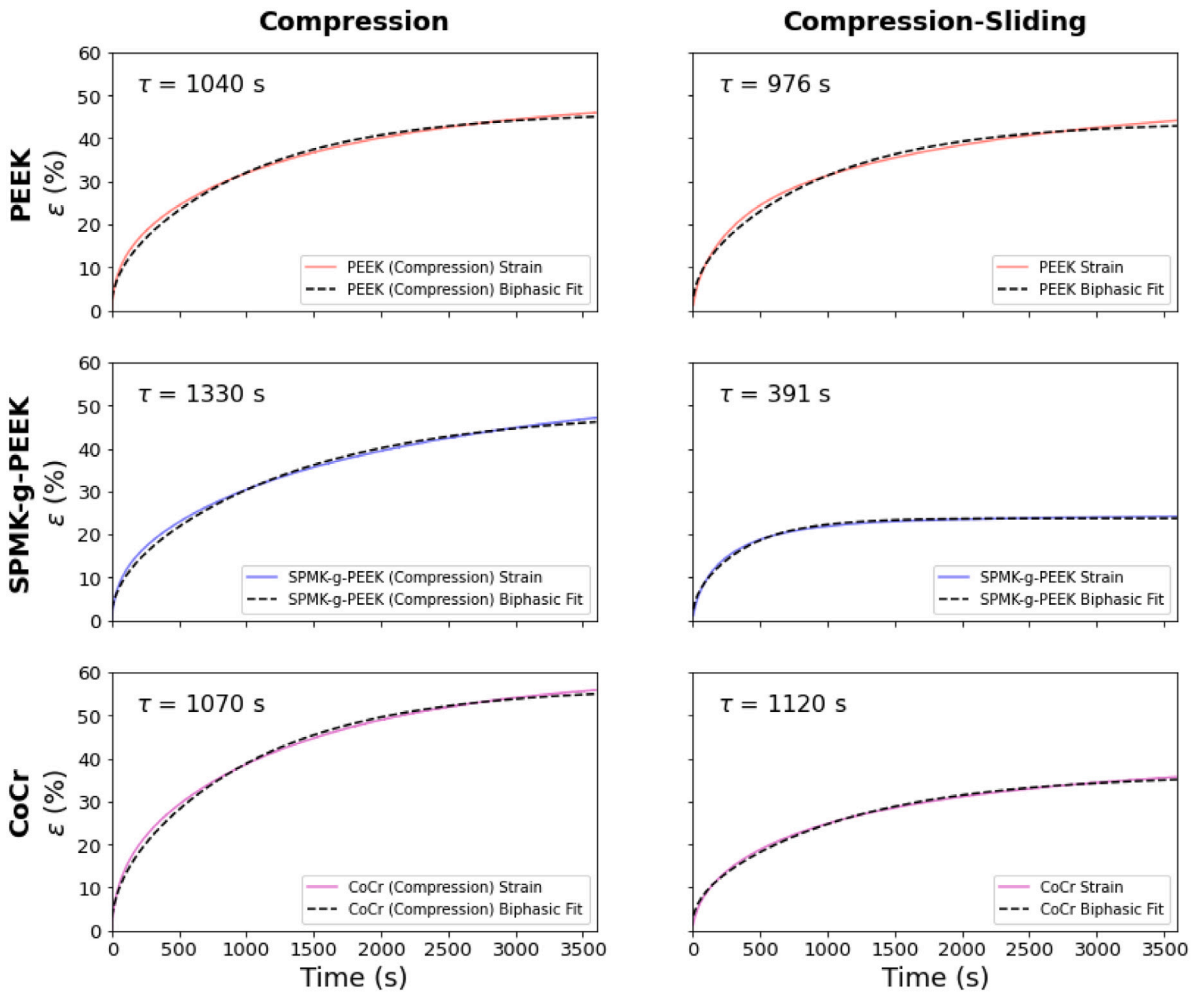

Fig. 9. Fitting of the biphasic theory model (Eq. (3)) to the first hour (t < 3600 s) of the cartilage during the Compression and Compression Sliding experiments for PEEK, SPMK-g-PEEK and CoCr. The biphasic time constant (τ) is annotated for each experiment.

calculated by fitting the biphasic strain equation of the characteristic time constant τ_c, the quality of the biphasic fit R^2, and the final strain after the 3600 s period of analysis $\varepsilon(t = 3600\ \text{s})$.

Cartilage sliding against PEEK and CoCr surfaces yielded τ_c of 976 s and 1120 s respectively, which are both within 10% of the corresponding compression control experiments (τ_c = 1040 s and 1070 s respectively), and hence indicate little evidence of altered interstitial fluid exudation during sliding. Early experiments designed to probe the viscoelastic properties of cartilage in compression consistently demonstrate the time to reaching equilibrium strain to be in excess of 1000 s and align with the CoCr and PEEK data presented in Table 4 (Coletti et al., 1972; Mow et al., 1980).

SPMK-g-PEEK surfaces reached the lowest equilibrium strain in a significantly shorter time with τ_c = 391 s, demonstrating that the effective permeability of the interfacing cartilage increases (Eq. (5)). Interestingly, the corresponding compression control for SPMK-g-PEEK yields an increased time constant of τ_c = 1330 s compared to the unfunctionalised PEEK control, implying a reduced interfacial permeability. Finite Element Analysis modelling of polyelectrolytes adsorbed on the cartilage surface predict that permeability is reduced by the presence of a polymer brush border (Liao et al., 2022). This contradiction demonstrates firstly that cartilage rehydration is triggered by sliding, and secondly the most likely explanation for the reduced equilibrium strain and short time constant during sliding is due to a competitive exudation–rehydration fluid flow.

In order to analyse the steadier approaching equilibrium strain, a linear regression (Eq. (7)) is fitted to the strain response in the final 90 min of the test (3600 s ≤ t ≤ 9000 s). In this final time period cartilage will be approaching the maximum equilibrium strain ($\varepsilon_{equilibrium}$), such that the gradient of the linear regression (β, Eq. (8)) will express the rate of change of strain and subsequently the sample propensity to maintain a stable strain equilibrium.

Table 4
Time constant τ_c are calculated by fitting the biphasic theory model (Eq. (3)) to the first 60 min (t < 3600 s) of strain data in Fig. 9. R^2 scores the quality of fit using Eq. (6). Strain at t = 3600 s is also given along with the ratio against final strain after 9000 s of Compression/Compression-Sliding (ε_{max}).

Sample	Compression			Compression-Sliding		
	τ_c	R^2	ε (t = 3600 s)	τ_c	R^2	ε (t = 3600 s)
PEEK	1040	0.994	45.9 (92% ε_{max})	976	0.992	44.1 (84% ε_{max})
SPMK-g-PEEK	1330	0.995	47.1 (86% ε_{max})	391	0.992	24.2 (92% ε_{max})
CoCr	1070	0.996	55.9 (94% ε_{max})	1120	0.997	35.7 (90% ε_{max})

$$\varepsilon_{equilibrium}(t) = \alpha + \beta t \qquad \text{for} \qquad t \geq 3600\ \text{s} \tag{7}$$

$$\beta = \frac{\sum_{i=3600}^{9000} (t_i - \bar{t})(\varepsilon_i - \bar{\varepsilon})}{\sum_{i=3600}^{9000} (t_i - \bar{t})^2} \tag{8}$$

Fig. 10 shows the long term creep behaviour and subsequent cartilage equilibrium strain rate by fitting a linear regression (Eq. (8)) to the strain response in the final 90 min (3600 s ≤ t ≤ 9000 s) of testing. Table 5 summarises the slope of the linear regression (β) expressed as

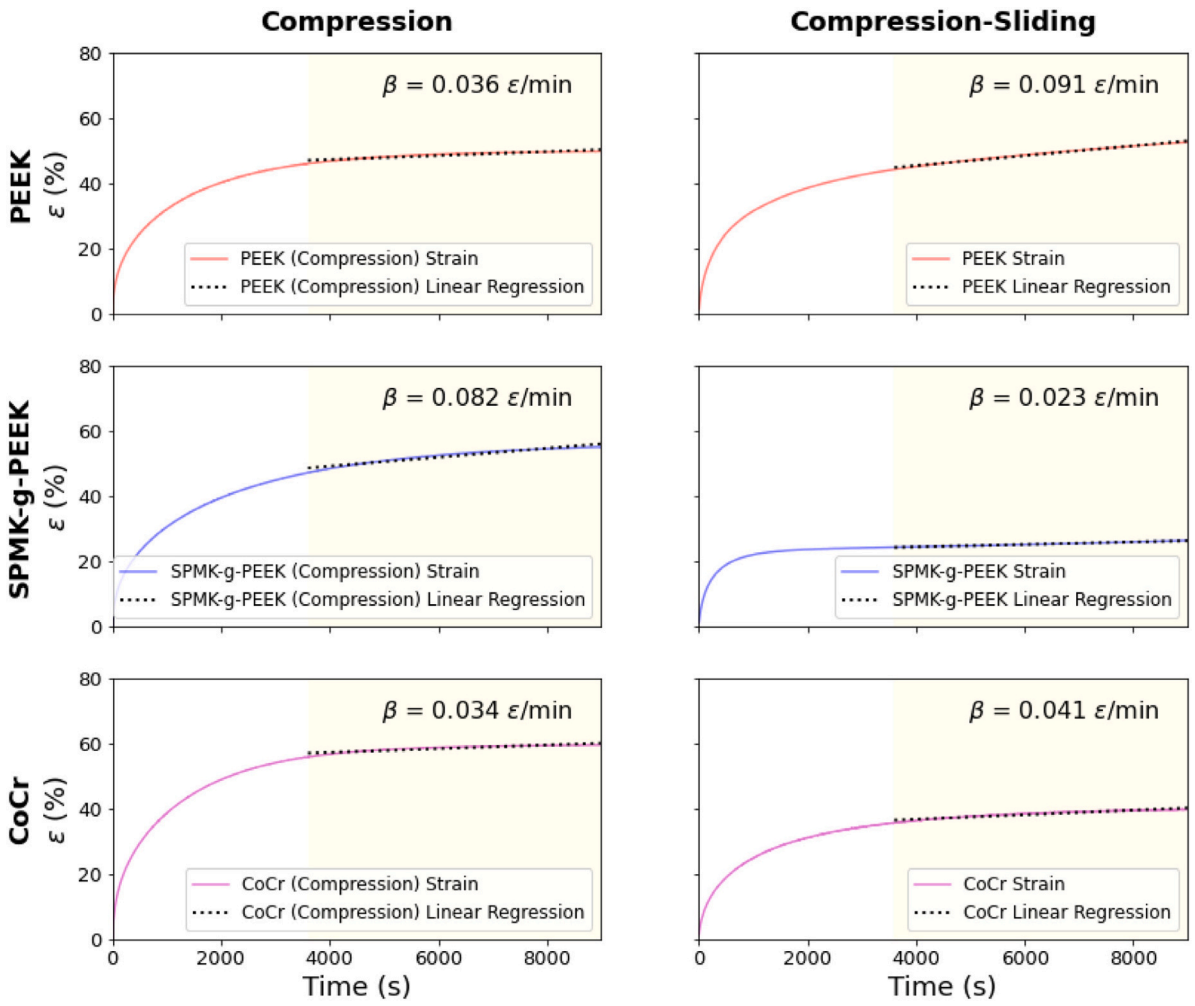

Fig. 10. Linear regression (Eq. (8)) fitted to the final 90 min (3600 s ≤ t ≤ 9000 s) of Compression and Compression-Sliding tests against PEEK, SPMK-g-PEEK and CoCr. The strain rate for this period β is annotated in terms of ϵ (%) / minute.

Table 5
Slope of the linear regression (β, Eq. (8)) given as increase in Strain (%)/min, and R^2 quality of fit score.

Sample	Compression		Compression-Sliding	
	β, Strain (%)/min	R^2	β, Strain (%)/min	R^2
PEEK (n = 4)	3.6 $\times 10^{-2}$	0.941	9.1 $\times 10^{-2}$	0.996
SPMK-g-PEEK (n = 4)	8.2 $\times 10^{-2}$	0.971	2.3 $\times 10^{-2}$	0.997
CoCr (n = 3)	3.4 $\times 10^{-2}$	0.926	4.1 $\times 10^{-2}$	0.941

increase in strain per minute and the coefficient of determination R^2 quality of linear regression fit.

The equilibrium cartilage strain creep behaviour for each test can be directly compared through the approximated linear strain rate (β) during the final phase of each test (3600 s ≤ t ≤ 9000 s). Sliding cartilage against SPMK-g-PEEK demonstrated the most favourable behaviour, with the lowest strain rate of 0.023 ϵ/minute, indicating the most effective progression towards an equilibrium strain state. Throughout compression-sliding tests the physics of fluid exudation of cartilage remain unchanged, thus the reduced creep indicates a competitive rehydration mechanism facilitated by the SPMK interface.

Cartilage sliding against PEEK yielded the highest strain rate of 0.091 ϵ/minute, indicating the greatest depletion of interstitial fluid and failure to approach a steady equilibrium value. This could be attributed to the ongoing breakdown of the collagen matrix due to high shear forces, as evidenced by observed surface damage and fibrillation (Fig. 8). Ultimately, such degradation would lead to reduced mechanical strength and reduced water retention capacity of cartilage.

Sliding strain rates for CoCr and the unconfined compression control exhibited comparable rates of 0.034 and 0.041 ϵ/minute respectively. These rates align the performance of CoCr closer to a balanced state, falling between the extremes of the SPMK-g-PEEK and PEEK. While SPMK-g-PEEK demonstrated a favourable progression towards an equilibrium strain state, and PEEK showed a tendency towards fluid depletion and collagen breakdown, CoCr's behaviour represents a moderate response that neither excels in rehydration nor fails in maintaining interstitial fluid as observed by the overall reduced strain. The strain rates for CoCr provides further insight into its tribological efficacy as a biomaterial for use in articulation against cartilage, and subsequent affinity to maintain fluid load support and improved lubricity compared to PEEK.

SPMK-g-PEEK samples exhibited a remarkably reduced biphasic time constant during sliding (τ_c = 391 s, over a 60% reduction compared to the unconfined compression control) and the minimal long term strain rate (β = 0.023 ϵ/minute). Cartilage rehydration is onset by sliding, akin to *tribological rehydration* profiled by Burris and

Moore (Voinier et al., 2022; Burris and Moore, 2017; Moore and Burris, 2017; Kupratis et al., 2021). Nonetheless, unlike previous investigations illustrating tribological rehydration that necessitates velocities surpassing 30 mms^{-1} and a convergent wedge configuration to generate adequate hydrodynamic pressures for cartilage rehydration, this study introduces a distinct mechanism of tribological rehydration that is independent of hydrodynamics (Voinier et al., 2022). This is achieved through the use of a compliant wetting surface, the hydrophilic and hydrated nature of the SPMK layer provides a means to deliver water and replenish water at the cartilage interface, promoting and maintaining hydration.

We hypothesise that during compression, polymer brushes may generate a high fluid pressure caused by the intensified excluded volume between polymer chains. This increased excluded volume leads to an augmented osmotic pressure within the brush interface, resulting in elevated fluid pressure (Chen et al., 2015). It is conjectured that if the osmotic pressure within the polymer brush is greater than the interstitial fluid pressure of cartilage, it could drive the flow of fluid back into the cartilage, thereby maintaining a greater proportion of fluid load support during sliding and reduced equilibrium strain.

4.3. Limitations and future work

Validity of biphasic model

Fitting the biphasic model (Eq. (3)) to the total strain response for each sample (Fig. 7) over the full 9000 s tests was unsuitable for PEEK and SPMK where the long term creep did not strictly follow an exponential decay with a single time constant. Hence the biphasic model was only fit to the first 3600 s of sliding tests where the contact strain is dominated by the time dependent biphasic fluid flow out of cartilage. A linear fit (Eq. (8)) was then used to model to the long term creep. Both of these metrics then enabled direct comparison of time dependent strain during sliding tests to the expected behaviour of cartilage in unconfined compression.

During the creep towards equilibrium strain phase (t > 3600 s) PEEK exhibited the greatest creep rate and final strain which reflects the tearing observed on the cartilage surface analysis following testing. During sliding tearing of the cartilage surface will both affect the real contact area and alter the aggregate modulus of the cartilage, which are assumed to be constant when modelling biphasic theory.

The biphasic model utilised in this study, initially introduced by Van Mow (Mow et al., 1980) and later expanded upon by Armstrong et al. (1984), offers a one dimensional solution that describes the temporal creep response of cartilage under confined and unconfined compression. However, this model does not consider material deformations resulting from shear forces at the interface during sliding. In the context of this study, the biphasic model is employed to examine the characteristic time constant associated with cartilage creep equilibrium, as has been done in previous research involving the assessment of in vivo cartilage mechanical function using MRI data (Cutcliffe et al., 2020).

To further elucidate the temporal behaviour of interstitial fluid pressure in cartilage during sliding and investigate the impact of polymer brush interfaces, future studies should employ constitutive models that incorporate cartilage poroelastic lubrication mechanisms. These advanced models will provide a more comprehensive understanding of how the pressure of the cartilage interstitial fluid is influenced by polymer brush interfaces over time (De Boer et al., 2020).

Further insight into polyelectrolyte interactions

The contact dynamics between two polyelectrolyte surfaces have previously demonstrated that steric repulsion between opposing brushy interfaces entropically favours a liquid interface to regulate polyelectrolyte interpenetration between opposing surfaces (Zappone et al., 2007; Iuster et al., 2017). In the experiments presented within this study, a polyelectrolyte functionalised surface could be expected to favourably interact with the macromolecules on the cartilage plug samples, however following harvesting all samples were washed with PBS which has been shown to disrupt and remove the natural boundary lubricating layer (Zappone et al., 2007). Further investigations into the interactions between synthesised polyelectrolyte surfaces (SPMK-g-PEEK) and synovial surfaces will provide additional insights into the beneficial interactions of SPMK functionalised biomaterials for their application in focal cartilage defect repair.

While this study provides valuable insights into the tribological properties of SPMK-g-PEEK and the supported cartilage fluid load bearing capacity, it has certain limitations that merit further investigation to fully elucidate fluid rehydration mechanisms at play. One limitation is the lack of direct measurements of cartilage interstitial fluid pressure during sliding. Future work should explore experimental setups to monitor interstitial fluid pressure in real-time, providing a more comprehensive understanding of the fluid load bearing capacity of the interfaces. Additionally, the long-term durability of SPMK-g-PEEK surfaces under physiologically representative conditions warrants investigation to assess their potential clinical applications.

5. Conclusions

This study demonstrates that surfaces functionalised with SPMK-g-PEEK exhibit tribological characteristics associated with effective hydration lubrication (evidenced by high wettability and the lowest coefficient of friction) and favourable modulation of interstitial fluid pressure (indicated by the lowest equilibrium strain (ε_{max}), equilibrium strain rate (β), and characteristic time constant (τ_c)). These findings align with the two main mechanisms that contribute to the high lubricity and longevity of healthy cartilage in synovial joints: hydration lubrication and sustained biphasic fluid load support (Katta et al., 2007; Jahn et al., 2016).

The following four key conclusions demonstrate the efficacy of SPMK-g-PEEK:

1. Hydrophilic Surface Coating: The one-step grafting procedure successfully creates a highly hydrophilic SPMK-g-PEEK surface, enabling effective hydration lubrication. This coating demonstrates the ability to sustain a low coefficient of friction (μ) during startup and sliding equilibrium against cartilage, with μ maintained below 0.024.

2. Minimised Cartilage Equilibrium Strain: SPMK-g-PEEK surfaces exhibit the ability to significantly reduce cartilage equilibrium strain. Facilitating the retention of a higher proportion of interstitial fluid and enhanced fluid load support compared to untreated biomaterials.

3. Effective Fluid Load Support: The improved fluid load support is attributed to the reduced effective cartilage permeability and the subsequent rehydration of cartilage initiated by sliding against SPMK-g-PEEK.

4. Novel Tribological Rehydration: Unlike previous models, which require specific conditions for hydrodynamic pressure-induced rehydration, SPMK-g-PEEK introduces a new mode of tribological rehydration. This polymer brush enabled mechanism operates independently of hydrodynamics, underscoring the capability of the surface to facilitate fluid delivery to the cartilage interface.

In conclusion, SPMK-g-PEEK surfaces emerge as a promising candidate for the next generation of osteochondral defect repairs, aiming to promote functional and healthy cartilage. The combination of hydration lubrication and sustained biphasic fluid load support allows these surfaces to mitigate damage, alleviate excessive loading on the collagen

matrix, and support cartilage biphasic viability. Created through a one-step grafting process, this highly hydrophilic and sterile surface coating offers benefits that include enhanced lubrication, maintained hydration, and prevention of cartilage damage. Future research should hone in on the long-term durability of SPMK-g-PEEK under physiologically representative conditions, the exploration of innovative focal repair device concepts, and the development of improved patient treatment pathways, thereby unlocking its full potential in supporting the health of interfacing cartilage.

CRediT authorship contribution statement

Robert J. Elkington: Writing – review & editing, Writing – original draft, Visualization, Validation, Resources, Methodology, Investigation, Formal analysis, Data curation, Conceptualization. **Richard M. Hall:** Writing – review & editing, Supervision. **Andrew R. Beadling:** Writing – review & editing. **Hemant Pandit:** Writing – review & editing, Supervision, Funding acquisition, Conceptualization. **Michael G. Bryant:** Writing – review & editing, Writing – original draft, Supervision, Methodology, Investigation, Funding acquisition, Formal analysis, Conceptualization.

Declaration of competing interest

The authors declare the following financial interests/personal relationships which may be considered as potential competing interests: Robert Elkington reports financial support was provided by UK Research and Innovation.

Data availability

The data associated with this paper is openly available from the Mendeley Data repository. Available: Elkington, Rob (2023), "Highly lubricious SPMK-g-PEEK implant surfaces to facilitate rehydration of articular cartilage", Mendeley Data, V1, doi: 10.17632/25bhnmxt82.1

Acknowledgements

Funding for this project was received from the UKRI Engineering and Physical Sciences Research Council.

The authors acknowledge the support and funding of the Bragg Centre for Materials Research at the University of Leeds, United Kingdom.

Professor Pandit is a National Institute for Health Research (NIHR) Senior Investigator. This study/research is funded by the NIHR Leeds Biomedical Research Centre (BRC). The views expressed are those of the author(s) and not necessarily those of the NIHR or the Department of Health and Social Care.

The authors acknowledge the support and funding of Friction: The Tribology Enigma which is funded by the Engineering and Physical Sciences Research Council, under grant no. EP/R001766/1.

Creative commons

References

Adams, D., Swanson, S.A., 1985. Direct measurement of local pressures in the cadaveric human hip joint during simulated level walking. Ann. Rheumat. Dis. 44 (10), 658–666. http://dx.doi.org/10.1136/ard.44.10.658.

Adenikinju, A., Slover, J.D., Egol, K.A., 2019. Rapid acetabular chondrolysis following hemiarthroplasty of the hip: A poor prognostic sign. Case Rep. Orthop. 2019, 1–8. http://dx.doi.org/10.1155/2019/7328526.

Armstrong, C.G., Lai, W.M., Mow, V.C., 1984. An analysis of the unconfined compression of articular cartilage. J. Biomech. Eng. 106 (2), 165–173. http://dx.doi.org/10.1115/1.3138475.

Armstrong, C., Mow, V.C., 1982. Variations in the intrinsic mechanical properties of human articular cartilage with age, degeneration, and water content. J. Bone Joint Surg.. Am. Vol. 64 (1), 88–94.

Ateshian, G.A., 1997. A theoretical formulation for boundary friction in articular cartilage. J. Biomech. Eng. 119 (1), 81–86. http://dx.doi.org/10.1115/1.2796069.

Bayliss, L.E., Culliford, D., Monk, A.P., Glyn-Jones, S., Prieto-Alhambra, D., Judge, A., Cooper, C., Carr, A.J., Arden, N.K., Beard, D.J., et al., 2017. The effect of patient age at intervention on risk of implant revision after total replacement of the hip or knee: A population-based cohort study. Lancet 389 (10077), 1424–1430.

Biresaw, G., 2013. Surfactants in Tribology, Volume 3. CRC Press.

Brand, R.A., 2005. Joint contact stress: A reasonable surrogate for biological processes? Iowa orthop. J. 25, 82.

Burris, D.L., Moore, A.C., 2017. Cartilage and joint lubrication: New insights into the role of hydrodynamics. Biotribology 12 (September), 8–14. http://dx.doi.org/10.1016/j.biotri.2017.09.001.

Burris, D., Ramsey, L., Graham, B., Price, C., Moore, A., 2019. How sliding and hydrodynamics contribute to articular cartilage fluid and lubrication recovery. Tribol. Lett. 67, 1–10.

Chan, S.M., Neu, C.P., Komvopoulos, K., Reddi, A.H., Di Cesare, P.E., 2011. Friction and wear of hemiarthroplasty biomaterials in reciprocating sliding contact with articular cartilage. J. Tribol. 133 (4), 1–7. http://dx.doi.org/10.1115/1.4004760.

Chen, M., Briscoe, W.H., Armes, S.P., Cohen, H., Klein, J., 2007. Robust, biomimetic polymer brush layers grown directly from a planar mica surface. ChemPhysChem 8 (9), 1303–1306.

Chen, C., Tang, P., Qiu, F., Shi, A.-C., 2015. Excluded volume effects in compressed polymer brushes: A density functional theory. J. Chem. Phys. 142 (12), 124904.

Chouwatat, P., Hirai, T., Higaki, K., Higaki, Y., Sue, H.J., Takahara, A., 2017. Aqueous lubrication of poly(etheretherketone) via surface-initiated polymerization of electrolyte monomers. Polymer 116, 549–555. http://dx.doi.org/10.1016/j.polymer.2017.02.085.

Clarke, I.C., Contini, R., Kenedi, R.M., 1974. Friction and wear studies of articular cartilage: A scanning electron microscopic study. Am. Soc. Mech. Eng. (Paper) (74-Lub-37), 358–366.

Coletti, Jr., J.M., Akeson, W.H., Woo, S.L., 1972. A comparison of the physical behavior of normal articular cartilage and the arthroplasty surface. J. Bone Joint Surg. 54 (1), 147–160.

Conzen, A., Eckstein, F., 2000. Quantitative determination of articular pressure in the human shoulder joint. J. Shoulder Elbow Surg. 9 (3), 196–204. http://dx.doi.org/10.1067/mse.2000.105137.

Curl, W.W., Krome, J., Gordon, E.S., Rushing, J., Smith, B.P., Poehling, G.G., 1997. Cartilage injuries: A review of 31,516 knee arthroscopies. Arthroscopy: J. Arthrosc. Related Surg. 13 (4), 456–460.

Custers, R., Dhert, W., Saris, D.B., Verbout, A., van Rijen, M., Mastbergen, S., Lafeber, F., Creemers, L., 2010. Cartilage degeneration in the goat knee caused by treating localized cartilage defects with metal implants. Osteoarthr. Cartil. 18 (3), 377–388.

Cutcliffe, H.C., Davis, K.M., Spritzer, C.E., DeFrate, L., 2020. The characteristic recovery time as a novel, noninvasive metric for assessing in vivo cartilage mechanical function. Ann. Biomed. Eng. 48 (12), 2901–2910.

De Boer, G., Raske, N., Soltanahmadi, S., Bryant, M., Hewson, R., 2020. Compliant-poroelastic lubrication in cartilage-on-cartilage line contacts. Tribol.-Mater., Surf. Interfaces 14 (3), 151–165.

de Boer, G.N., Raske, N., Soltanahmadi, S., Dowson, D., Bryant, M.G., Hewson, R.W., 2020. A porohyperelastic lubrication model for articular cartilage in the natural synovial joint. Tribol. Int. 149 (May 2019), 105760. http://dx.doi.org/10.1016/j.triboint.2019.04.044.

Dedinaite, A., 2012. Biomimetic lubrication. Soft Matter http://dx.doi.org/10.1039/c1sm06335a.

Diermeier, T., Venjakob, A., Byrne, K., Burgkart, R., Foehr, P., Milz, S., Imhoff, A.B., Vogt, S., 2020. Effects of focal metallic implants on opposing cartilage–An in-vitro study with an abrasion test machine. BMC Musculoskelet. Disord. 21 (1), 1–7.

Dowson, D., Unsworth, A., Wright, V., 1975. The finctional behavior of human synovial joints-part I: Natural joints. (july). pp. 369–376.

Eichenbaum, G., Wilsey, J.T., Fessel, G., Qiu, Q.-Q., Perkins, L., Hasgall, P., Monnot, A., More, S.L., Egnot, N., Sague, J., et al., 2021. An integrated benefit-risk assessment of cobalt-containing alloys used in medical devices: Implications for regulatory requirements in the European union. Regul. Toxicol. Pharmacol. 125, 105004.

Elkington, R., Beadling, A., Hall, R., Pandit, H., Bryant, M., 2021. Biomimetic highly lubricious polyelectrolyte functionalized peek surfaces for novel hemiarthroplasty implants and focal resurfacing. In: Orthopaedic Proceeding, vol. 103, (no. SUPP_16), The British Editorial Society of Bone & Joint Surgery, p. 34.

Forster, H., Fisher, J., 1999. The influence of continuous sliding and subsequent surface wear on the friction of articular cartilage. Proc. Inst. Mech. Eng., Part H: J. Eng. Med. 213 (4), 329–345. http://dx.doi.org/10.1243/0954411991535167.

Goda, T., Konno, T., Takai, M., Moro, T., Ishihara, K., 2006. Biomimetic phosphorylcholine polymer grafting from polydimethylsiloxane surface using photo-induced polymerization. Biomaterials 27 (30), 5151–5160.

Hangody, L., Füles, P., 2003. Autologous osteochondral mosaicplasty for the treatment of full-thickness defects of weight-bearing joints: Ten years of experimental and clinical experience. J. Bone Joint Surg. 85 (suppl_2), 25–32.

Hjelle, K., Solheim, E., Strand, T., Muri, R., Brittberg, M., 2002. Articular cartilage defects in 1,000 knee arthroscopies. Arthroscopy: J. Arthrosc. Related Surg. 18 (7), 730–734.

Hodge, W.A., Harris, W.H., 1986. Contact pressures in the human hip joint measured in vivo, vol. 83 (May). pp. 2879–2883.

Ishihara, K., 2015a. Highly lubricated polymer interfaces for advanced artificial hip joints through biomimetic design. Polym. J. 47 (9), 585–597. http://dx.doi.org/10.1038/pj.2015.45.

Ishihara, K., 2015b. Highly lubricated polymer interfaces for advanced artificial hip joints through biomimetic design, no. March. (ISSN: 0032-3896) pp. 1–13. http://dx.doi.org/10.1038/pj.2015.45.

Ishihara, K., 2022. Biomimetic materials based on zwitterionic polymers toward human-friendly medical devices. Sci. Technol. Adv. Mater. 23 (1), 498–524.

Iuster, N., Tairy, O., Driver, M.J., Armes, S.P., Klein, J., 2017. Cross-linking highly lubricious phosphocholinated polymer brushes: Effect on surface interactions and frictional behavior. Macromolecules 50 (18), 7361–7371. http://dx.doi.org/10.1021/acs.macromol.7b01423.

Jahn, S., Klein, J., 2015. Hydration lubrication: The macromolecular domain. Macromolecules 48 (15), 5059–5075. http://dx.doi.org/10.1021/acs.macromol.5b00327.

Jahn, S., Klein, J., 2018. Lubrication of articular cartilage. Phys. Today 48 (71), http://dx.doi.org/10.1063/PT.3.3898.

Jahn, S., Seror, J., Klein, J., 2016. Lubrication of articular cartilage. Ann. Rev. Biomed. Eng. 18, 235–258.

Jermin, P., Yates, J., McNicholas, M., 2015. (vi) focal resurfacing implants in the knee and partial knee replacements. Orthop. Trauma 29 (1), 38–47.

Katta, J., Pawaskar, S., Jin, Z., Ingham, E., Fisher, J., 2007. Effect of load variation on the friction properties of articular cartilage. Proc. Inst. Mech. Eng., Part J: J. Eng. Tribol. 221 (3), 175–181.

Kim, Y.S., Kim, Y.H., Hwang, K.T., Choi, I.Y., 2012. The cartilage degeneration and joint motion of bipolar hemiarthroplasty. Int. Orthop. 36 (10), 2015–2020. http://dx.doi.org/10.1007/s00264-012-1567-9.

Kobayashi, M., Takahara, A., 2010. Tribological properties of hydrophilic polymer brushes under wet conditions. Chem. Rec. 10 (4), 208–216. http://dx.doi.org/10.1002/tcr.201000001.

Kobayashi, M., Takahara, A., 2012. Polyelectrolyte brushes : A novel stable lubrication system in aqueous conditions. pp. 403–412. http://dx.doi.org/10.1039/c2fd00123c.

Krishnan, R., Kopacz, M., Ateshian, G.A., 2004. Experimental verification of the role of interstitial fluid pressurization in cartilage lubrication. J. Orthop. Res. 22 (3), 565–570. http://dx.doi.org/10.1016/j.orthres.2003.07.002.

Kupratis, M.E., Gure, A.E., Ortved, K.F., Burris, D.L., Price, C., 2021. Comparative tribology: Articulation-induced rehydration of cartilage across species. Biotribology 25, 100159.

Kyomoto, M., Moro, T., Saiga, K.-i., Miyaji, F., Kawaguchi, H., 2010a. Lubricity and stability of poly (2-methacryloyloxyethyl phosphorylcholine) polymer layer on Co – Cr – Mo surface for hemi-arthroplasty to prevent degeneration of articular cartilage. Biomaterials 31 (4), 658–668. http://dx.doi.org/10.1016/j.biomaterials.2009.09.083.

Kyomoto, M., Moro, T., Takatori, Y., Kawaguchi, H., Nakamura, K., Ishihara, K., 2010b. Self-initiated surface grafting with poly(2-methacryloyloxyethyl phosphorylcholine) on poly(ether-ether-ketone). Biomaterials 31 (6), 1017–1024. http://dx.doi.org/10.1016/j.biomaterials.2009.10.055.

Kyomoto, M., Moro, T., Takatori, Y., Tanaka, S., Ishihara, K., 2015. Multidirectional wear and impact-to-wear tests of phospholipid-polymer-grafted and vitamin E-blended crosslinked polyethylene: a pilot study. Clin. Orthop. Relat. Res. 473, 942–951.

Lanigan, J.L., Fatima, S., Charpentier, T.V., Neville, A., Dowson, D., Bryant, M., 2018. Lubricious ionic polymer brush functionalised silicone elastomer surfaces. Biotribology 16 (March), 1–9. http://dx.doi.org/10.1016/j.biotri.2018.08.001.

Law, K.-Y., 2014. Definitions for hydrophilicity, hydrophobicity, and superhydrophobicity: Getting the basics right. J. Phys. Chem. Lett. 5 (4), 686–688.

Liao, J., Smith, D.W., Miramini, S., Gardiner, B.S., Zhang, L., 2022. Investigation of role of cartilage surface polymer brush border in lubrication of biological joints. Friction 10 (1), 110–127.

Lin, W., Klein, J., 2019. Control of surface forces through hydrated boundary layers. Curr. Opin. Colloid Interface Sci. 44, 94–106.

Lin, W., Klein, J., 2022. Hydration lubrication in biomedical applications: From cartilage to hydrogels. Accounts Mater. Res. 3 (2), 213–223.

Liu, G., Liu, Z., Li, N., Wang, X., Zhou, F., Liu, W., 2014. Hairy polyelectrolyte brushes-grafted thermosensitive microgels as artificial synovial fluid for simultaneous biomimetic lubrication and arthritis treatment. ACS Appl. Mater. Interfaces 6 (22), 20452–20463.

Mabuchi, K., Tsukamoto, Y., Obara, T., Yamaguchi, T., 1994. The effect of additive hyaluronic acid on animal joints with experimentally reduced lubricating ability. J. Biomed. Mater. Res. 28 (8), 865–870. http://dx.doi.org/10.1002/jbm.820280805.

Meehan, J.P., Danielsen, B., Kim, S.H., Jamali, A.A., White, R.H., 2014. Younger age is associated with a higher risk of early periprosthetic joint infection and aseptic mechanical failure after total knee arthroplasty. J. Bone Joint Surg. 96 (7), 529–535.

Mocny, P., Klok, H.A., 2016. Tribology of surface-grafted polymer brushes. Mol. Syst. Des. Eng. 1 (2), 141–154. http://dx.doi.org/10.1039/c5me00010f.

Mollon, B., Kandel, R., Chahal, J., Theodoropoulos, J., 2013. The clinical status of cartilage tissue regeneration in humans. Osteoarthritis Cartilage 21 (12), 1824–1833.

Moore, A.C., Burris, D.L., 2017. Tribological rehydration of cartilage and its potential role in preserving joint health. Osteoarthr. Cartil. 25 (1), 99–107. http://dx.doi.org/10.1016/j.joca.2016.09.018.

Moore, A.C., Schrader, J.L., Ulvila, J.J., Burris, D.L., 2017. A review of methods to study hydration effects on cartilage friction. Tribol.-Mater., Surf. Interfaces 11 (4), 202–214.

Mow, V.C., Kuei, S., Lai, W.M., Armstrong, C.G., 1980. Biphasic creep and stress relaxation of articular cartilage in compression: Theory and experiments. J. Biomech. Eng. 102 (1), 73–84.

Nakano, H., Noguchi, Y., Kakinoki, S., Yamakawa, M., Osaka, I., Iwasaki, Y., 2020. Highly durable lubricity of photo-cross-linked zwitterionic polymer brushes supported by poly(ether ether ketone) substrate. http://dx.doi.org/10.1021/acsabm.9b01040.

Northwood, E., Fisher, J., 2007. A multi-directional in vitro investigation into friction, damage and wear of innovative chondroplasty materials against articular cartilage. Clin. Biomech. 22 (7), 834–842.

Pawaskar, S.S., Ingham, E., Fisher, J., Jin, Z., 2011. Fluid load support and contact mechanics of hemiarthroplasty in the natural hip joint. Med. Eng. Phys. 33 (1), 96–105. http://dx.doi.org/10.1016/j.medengphy.2010.09.009.

Pawlak, Z., Urbaniak, W., Oloyede, A., 2011. The relationship between friction and wettability in aqueous environment. Wear 271 (9–10), 1745–1749.

Roberts, B.J., Unsworth, A., Mian, N., 1982. Modes of lubrication in human hip joints. Ann. Rheum. Dis. 41 (3), 217–224. http://dx.doi.org/10.1136/ard.41.3.217.

Siddaiah, A., Menezes, P.L., 2016. Advances in bio-inspired tribology for engineering applications. J. Bio- Tribo-Corrosion 2 (4), 1–19.

Sophia Fox, A.J., Bedi, A., Rodeo, S.A., 2009. The basic science of articular cartilage: Structure, composition, and function. Sports Health 1 (6), 461–468. http://dx.doi.org/10.1177/1941738109350438.

Stewart, T.D., 2010. Tribology of artificial joints. Orthop. Trauma 24 (6), 435–440. http://dx.doi.org/10.1016/j.mporth.2010.08.002.

Stojanović, B., Bauer, C., Stotter, C., Klestil, T., Nehrer, S., Franek, F., Ripoll, M.R., 2019. Tribocorrosion of a CoCrMo alloy sliding against articular cartilage and the impact of metal ion release on chondrocytes. Acta Biomater. 94, 597–609.

Stormont, T.J., An, K.N., Morrey, B.F., Chao, E.Y., 1985. Elbow joint contact study: Comparison of techniques. J. Biomech. 18 (5), 329–336. http://dx.doi.org/10.1016/0021-9290(85)90288-X.

Tan, W.S., Moore, A.C., Stevens, M.M., 2023. Minimum design requirements for a poroelastic mimic of articular cartilage. J. Mech. Behav. Biomed. Mater. 137, 105528.

Unsworth, A., Dowson, D., Wright, V., 1975. Some new evidence on human joint lubrication. Ann. Rheumatic Dis. 34, 277–285.

Virtanen, P., Gommers, R., Oliphant, T.E., Haberland, M., Reddy, T., Cournapeau, D., Burovski, E., Peterson, P., Weckesser, W., Bright, J., et al., 2020. Scipy 1.0: Fundamental algorithms for scientific computing in Python. Nat. methods 17 (3), 261–272.

Voinier, S., Moore, A., Benson, J.M., Price, C., Burris, D.L., 2022. The modes and competing rates of cartilage fluid loss and recovery. Acta Biomater. 138, 390–397.

Willing, R., King, G.J., Johnson, J.A., 2015. Contact mechanics of reverse engineered distal humeral hemiarthroplasty implants. J. Biomech. 48 (15), 4037–4042. http://dx.doi.org/10.1016/j.jbiomech.2015.09.047.

Zappone, B., Ruths, M., Greene, G.W., Jay, G.D., Israelachvili, J.N., 2007. Adsorption, lubrication, and wear of lubricin on model surfaces: Polymer brush-like behavior of a glycoprotein. Biophys. J. 92 (5), 1693–1708. http://dx.doi.org/10.1529/biophysj.106.088799.